

VALIDATION OF CFD CODES FOR AERODYNAMIC ANALYSIS OF LAUNCH VEHICLES AND SOUNDING ROCKETS

Alexandre Noll Marques

Instituto Tecnológico de Aeronáutica
noll@h8.ita.br

João Luiz F. Azevedo

Instituto de Aeronáutica e Espaço
azevedo@iae.cta.br

João Roberto Barbosa

Instituto Tecnológico de Aeronáutica
barbosa@mec.ita.cta.br

Abstract. The present work describes the continuation of the validation process of a computational code which is able to simulate three-dimensional compressible flows with turbulent transport effects over realistic configurations of CTA/IAE's rockets. Systematic mesh refinement studies are performed in order to determine the optimal conditions for each case. New mesh topologies are created in an attempt to provide better grids for supersonic flow situations. Simulations are performed with the objective of contributing to the validation effort of the numerical simulation tool under development.

Keywords. *CFD, Aerodynamics, VLS, Sonda III-A.*

1. Introduction

Computational Fluid Mechanics (CFD) is an extremely important subject in present Aerodynamics. As described by Fletcher (1988), the mathematical modeling of the great majority of real aerodynamic phenomena comprises a system of nonlinear partial differential equations which is of difficult analytical manipulation. Up to the emergence of the first computational tools, these difficulties were overcome exclusively with exhaustive use of flight and wind tunnels tests.

However, Aerodynamics has reaped the benefits of computer developments over the past decades, as shown in Fletcher (1988). The present CFD tools are very flexible and are largely used in all aerospace industries due to the large savings they represent. Depending on the focused circumstances, one should give up of some irrelevant elements and concentrate all the efforts on the most interesting aspects to the result. Hirsch (1994) and Azevedo (1993) deal, among others subjects, with the question of simplifying the mathematical models to find more satisfactory solutions in specific cases.

The main variables involved in this case analysis are, besides the body's geometry, the Mach and Reynolds numbers. The first is directly related to the flow compressibility, while the second covers parameters such as velocity, density, viscosity and the vehicle's dimension.

After selection of the theoretical model, it is indispensable to define the physical domain where the flows take place, determining the boundary conditions to the problem. In order to treat the flows numerically, it is necessary to discretize the physical domain defining point locations over a computational mesh where the calculations are performed. This step, as stated by Fletcher (1988) and confirmed by the group at CTA/IAE, is extremely important for solution accuracy and convergence. Cases later discussed will make this more evident.

As presented by Marques (2002), together with the evolution of the projects performed at CTA/IAE, came the increasing need of aerodynamic parameters, mainly concerning the vehicles developed in that center. Nevertheless, the use of CFD tools has always been limited by the necessity of development of proper computational codes and computational resources compatible to the extension of the work. Hence, a progressive approach concerning the complexity was adopted in the development of such tools at CTA/IAE and ITA. Therefore, the stages described in the listed references were followed (Azevedo, 1990; Azevedo et al., 1995 and 1997; Fico and Azevedo, 1994; Bigarelli et al. 1999; Cruz, 2000 and Bigarelli; and Azevedo, 2002). After the most recent improvements in the code along the last two years, the actual tool solves three-dimensional problems with a Navier-Stokes formulation including viscosity and turbulent transport effects, as well as advanced convergence acceleration techniques, as stated by Bigarelli (2002).

Every numerical tool developed to obtain approximate solutions for mathematical problems must be validated. This process consists in extensive comparisons of results with independent computations available in the literature and experimental data. Although the long term objective is to achieve results which are similar to those well-known data, the most important aspect of this process to an engineer is to know the limitations of the tool he/she is using. This will guarantee the adequate utilization of the code and even make improvements possible. Hence, the main objective of the present work is to contribute towards the validation of the recently added capabilities to this CFD code under development. In particular, the work is concentrated on the definition of better mesh topologies for the problems of interest.

2. Theoretical Formulation

2.1. Mathematical Formulation

Based on Marques (2002), the actual code solves the thin layer approximation for three-dimensional, compressible, turbulent flows, based on the Reynolds averaged Navier-Stokes equations. These equations are presented in the conservative form for generalized curvilinear coordinates by Marques (2002) as follows

$$\frac{\partial \bar{Q}}{\partial \tau} + \frac{\partial \bar{E}}{\partial \xi} + \frac{\partial \bar{F}}{\partial \eta} + \frac{\partial \bar{G}}{\partial \zeta} = \frac{\partial \bar{E}_v}{\partial \xi} + \frac{\partial \bar{F}_v}{\partial \eta} + \frac{\partial \bar{G}_v}{\partial \zeta}, \quad (1)$$

where \bar{Q} is the conservative variables vector, given by Eq. (2).

$$\bar{Q} = J^{-1} [\rho \quad \rho u \quad \rho v \quad \rho w \quad e]^T. \quad (2)$$

The inviscid flux terms \bar{E} , \bar{F} and \bar{G} are defined as

$$\bar{E} = J^{-1} \begin{Bmatrix} \rho U \\ \rho uU + p\xi_x \\ \rho vU + p\xi_y \\ \rho wU + p\xi_z \\ (e+p)U - p\xi_x \end{Bmatrix}, \quad \bar{F} = J^{-1} \begin{Bmatrix} \rho V \\ \rho uV + p\eta_x \\ \rho vV + p\eta_y \\ \rho wV + p\eta_z \\ (e+p)V - p\eta_x \end{Bmatrix} \quad \text{and} \quad \bar{G} = J^{-1} \begin{Bmatrix} \rho W \\ \rho uW + p\zeta_x \\ \rho vW + p\zeta_y \\ \rho wW + p\zeta_z \\ (e+p)W - p\zeta_x \end{Bmatrix}, \quad (3)$$

and the viscous flux terms \bar{E}_v , \bar{F}_v and \bar{G}_v as

$$\bar{E}_v = J^{-1} \begin{Bmatrix} 0 \\ \xi_x \tau_{xx} + \xi_y \tau_{xy} + \xi_z \tau_{xz} \\ \xi_x \tau_{xy} + \xi_y \tau_{yy} + \xi_z \tau_{yz} \\ \xi_x \tau_{xz} + \xi_y \tau_{yz} + \xi_z \tau_{zz} \\ \xi_x \beta_x + \xi_y \beta_y + \xi_z \beta_z \end{Bmatrix}, \quad \bar{F}_v = J^{-1} \begin{Bmatrix} 0 \\ \eta_x \tau_{xx} + \eta_y \tau_{xy} + \eta_z \tau_{xz} \\ \eta_x \tau_{xy} + \eta_y \tau_{yy} + \eta_z \tau_{yz} \\ \eta_x \tau_{xz} + \eta_y \tau_{yz} + \eta_z \tau_{zz} \\ \eta_x \beta_x + \eta_y \beta_y + \eta_z \beta_z \end{Bmatrix} \quad \text{and} \quad \bar{G}_v = J^{-1} \begin{Bmatrix} 0 \\ \zeta_x \tau_{xx} + \zeta_y \tau_{xy} + \zeta_z \tau_{xz} \\ \zeta_x \tau_{xy} + \zeta_y \tau_{yy} + \zeta_z \tau_{yz} \\ \zeta_x \tau_{xz} + \zeta_y \tau_{yz} + \zeta_z \tau_{zz} \\ \zeta_x \beta_x + \zeta_y \beta_y + \zeta_z \beta_z \end{Bmatrix}. \quad (4)$$

In Eq. (4), ρ is the density; u , v and w are the Cartesian velocity components and e is the total internal energy per unity of volume. Considering the perfect gases equation, pressure can be written as

$$p = (\gamma - 1)\rho e_i = (\gamma - 1) \left[e - \frac{1}{2} \rho (u^2 + v^2 + w^2) \right], \quad (5)$$

where e_i is the specific internal energy and γ is the ratio of specific heats at constant pressure and constant volume. The components of the viscous stress tensor are described by the relations

$$\tau_{xx} = \frac{2}{3} \mu \left(2 \frac{\partial u}{\partial x} - \frac{\partial v}{\partial y} - \frac{\partial w}{\partial z} \right), \quad \tau_{yy} = \mu \left(\frac{\partial u}{\partial y} + \frac{\partial v}{\partial x} \right), \quad \tau_{zz} = \mu \left(\frac{\partial w}{\partial x} + \frac{\partial u}{\partial z} \right),$$

$$\tau_{xy} = \frac{2}{3} \mu \left(2 \frac{\partial v}{\partial y} - \frac{\partial u}{\partial x} - \frac{\partial w}{\partial z} \right), \quad \tau_{yz} = \mu \left(\frac{\partial v}{\partial z} + \frac{\partial w}{\partial y} \right) \quad \text{and} \quad \tau_{zx} = \frac{2}{3} \mu \left(2 \frac{\partial w}{\partial z} - \frac{\partial u}{\partial x} - \frac{\partial v}{\partial y} \right). \quad (6)$$

The terms above referenced as β_x , β_y and β_z are given by

$$\beta_x = \tau_{xx} u + \tau_{xy} v + \tau_{xz} w + q_x,$$

$$\beta_y = \tau_{yx} u + \tau_{yy} v + \tau_{yz} w + q_y,$$

$$\beta_z = \tau_{zx} u + \tau_{zy} v + \tau_{zz} w + q_z. \quad (7)$$

The contravariant velocity components are defined as

$$\begin{aligned} U &= \xi_t + \xi_x u + \xi_y v + \xi_z w, \\ V &= \eta_t + \eta_x u + \eta_y v + \eta_z w, \\ W &= \zeta_t + \zeta_x u + \zeta_y v + \zeta_z w. \end{aligned} \quad (8)$$

The q_x , q_y and q_z amounts are the heat flux components, given by

$$\vec{q} = -k\vec{\nabla}T. \quad (9)$$

In the present work, the Cartesian coordinates system adopted is the one with the x-axis in the vehicle's longitudinal direction, set as positive in the downstream sense. The others two coordinates complete the system according to the right-hand rule. The generalized curvilinear coordinate system is defined by ξ as the body longitudinal direction, η as the direction normal to the solid wall and ζ as the circumferential direction. This system is obtained by the following coordinate transformation

$$\begin{aligned} \tau &= t, \\ \xi &= \xi(x, y, z, t), \\ \eta &= \eta(x, y, z, t), \\ \zeta &= \zeta(x, y, z, t). \end{aligned} \quad (10)$$

The Jacobian of this transformation is given by Eq. (11), which is valid for the three-dimensional case

$$J = (x_\xi y_\eta z_\zeta + x_\eta y_\zeta z_\xi + x_\zeta y_\xi z_\eta - x_\xi y_\zeta z_\eta - x_\eta y_\xi z_\zeta - x_\zeta y_\eta z_\xi)^{-1}. \quad (11)$$

The ξ_x , ξ_y , ξ_z , ξ_t , η_x , η_y , η_z , η_t , ζ_x , ζ_y , ζ_z e ζ_t are the metric terms, while x_ξ , y_ξ , z_ξ , x_η , y_η , z_η , x_ζ , y_ζ , z_ζ , x_τ , y_τ e z_τ are the inverse metric terms. These first terms are

$$\begin{aligned} \xi_x &= J(y_\eta z_\zeta - y_\zeta z_\eta), \quad \xi_y = J(x_\zeta z_\eta - x_\eta z_\zeta), \quad \xi_z = J(x_\eta y_\zeta - x_\zeta y_\eta), \\ \eta_x &= J(y_\zeta z_\xi - y_\xi z_\zeta), \quad \eta_y = J(x_\xi z_\zeta - x_\zeta z_\xi), \quad \eta_z = J(x_\zeta y_\xi - x_\xi y_\zeta), \\ \zeta_x &= J(y_\xi z_\eta - y_\eta z_\xi), \quad \zeta_y = J(x_\eta z_\xi - x_\xi z_\eta), \quad \zeta_z = J(x_\xi y_\eta - x_\eta y_\xi), \\ \xi_t &= -x_\tau \xi_x - y_\tau \xi_y - z_\tau \xi_z, \quad \eta_t = -x_\tau \eta_x - y_\tau \eta_y - z_\tau \eta_z, \quad \zeta_t = -x_\tau \zeta_x - y_\tau \zeta_y - z_\tau \zeta_z. \end{aligned} \quad (12)$$

Developing the equations above cited and neglecting the crossed derivatives terms (Cruz, 2000), one can rewrite the viscous flux vectors as

$$\begin{aligned} \bar{E}_V &= J^{-1} \begin{bmatrix} 0 \\ \mu(\xi_x^2 + \xi_y^2 + \xi_z^2)u_\xi + (\mu/3)(\xi_x u_\xi + \xi_y v_\xi + \xi_z w_\xi)\xi_x \\ \mu(\xi_x^2 + \xi_y^2 + \xi_z^2)v_\xi + (\mu/3)(\xi_x u_\xi + \xi_y v_\xi + \xi_z w_\xi)\xi_y \\ \mu(\xi_x^2 + \xi_y^2 + \xi_z^2)w_\xi + (\mu/3)(\xi_x u_\xi + \xi_y v_\xi + \xi_z w_\xi)\xi_z \\ (\xi_x^2 + \xi_y^2 + \xi_z^2) \left[\frac{\mu}{2}(u^2 + v^2 + w^2)_\xi + kT_\xi \right] + \frac{\mu}{3}(\xi_x u + \xi_y v + \xi_z w)(\xi_x u_\xi + \xi_y v_\xi + \xi_z w_\xi) \end{bmatrix}, \\ \bar{F}_V &= J^{-1} \begin{bmatrix} 0 \\ \mu(\eta_x^2 + \eta_y^2 + \eta_z^2)u_\eta + (\mu/3)(\eta_x u_\eta + \eta_y v_\eta + \eta_z w_\eta)\eta_x \\ \mu(\eta_x^2 + \eta_y^2 + \eta_z^2)v_\eta + (\mu/3)(\eta_x u_\eta + \eta_y v_\eta + \eta_z w_\eta)\eta_y \\ \mu(\eta_x^2 + \eta_y^2 + \eta_z^2)w_\eta + (\mu/3)(\eta_x u_\eta + \eta_y v_\eta + \eta_z w_\eta)\eta_z \\ (\eta_x^2 + \eta_y^2 + \eta_z^2) \left[\frac{\mu}{2}(u^2 + v^2 + w^2)_\eta + kT_\eta \right] + \frac{\mu}{3}(\eta_x u + \eta_y v + \eta_z w)(\eta_x u_\eta + \eta_y v_\eta + \eta_z w_\eta) \end{bmatrix}, \end{aligned}$$

$$\bar{G}_V = J^{-1} \begin{bmatrix} 0 \\ \mu(\zeta_x^2 + \zeta_y^2 + \zeta_z^2)u_\zeta + (\mu/3)(\zeta_x u_\zeta + \zeta_y v_\zeta + \zeta_z w_\zeta)\zeta_x \\ \mu(\zeta_x^2 + \zeta_y^2 + \zeta_z^2)v_\zeta + (\mu/3)(\zeta_x u_\zeta + \zeta_y v_\zeta + \zeta_z w_\zeta)\zeta_y \\ \mu(\zeta_x^2 + \zeta_y^2 + \zeta_z^2)w_\zeta + (\mu/3)(\zeta_x u_\zeta + \zeta_y v_\zeta + \zeta_z w_\zeta)\zeta_z \\ (\zeta_x^2 + \zeta_y^2 + \zeta_z^2) \left[\frac{\mu}{2}(u^2 + v^2 + w^2)_\zeta + kT_\zeta \right] + \frac{\mu}{3}(\zeta_x u + \zeta_y v + \zeta_z w)(\zeta_x u_\zeta + \zeta_y v_\zeta + \zeta_z w_\zeta) \end{bmatrix}. \quad (13)$$

The Mach number, cited previously, is given by

$$M_\infty = \frac{U_\infty}{a_\infty}, \quad (14)$$

where U_∞ and a_∞ the freestream flow and sound velocities, respectively. Moreover, the other very important parameter Reynolds number is defined as

$$\text{Re} = \frac{\rho_\infty l_0 U_\infty}{\mu_\infty}, \quad (15)$$

where ρ_∞ and μ_∞ are the freestream density and the viscosity coefficient and l_0 is the reference length, which is, in the present work, the vehicle's diameter at the outflow boundary region.

2.2. Numerical Formulation

The basic equations have to be discretized for numerical treatment. The spatial derivatives are discretized with a centered difference scheme, while the time derivatives are represented by a five-stage Runge-Kutta time marching method of second order of accuracy, as described by Cruz (2000) and Azevedo (1989). As usual with centered difference schemes, artificial dissipation terms are added to maintain stability in nonlinear cases.

In the present code, the artificial dissipation terms are implemented modifying the convective fluxes as follows:

$$\begin{aligned} E_{i \pm 1/2, j, k} &= 1/2(\bar{E}_{i, j, k} + \bar{E}_{i \pm 1, j, k}) - 1/2(J_{i, j, k}^{-1} + J_{i \pm 1, j, k}^{-1})d_{i \pm 1/2, j, k}, \\ F_{i, j \pm 1/2, k} &= 1/2(\bar{F}_{i, j, k} + \bar{F}_{i, j \pm 1, k}) - 1/2(J_{i, j, k}^{-1} + J_{i, j \pm 1, k}^{-1})d_{i, j \pm 1/2, k}, \\ G_{i, j, k \pm 1/2} &= 1/2(\bar{G}_{i, j, k} + \bar{G}_{i, j, k \pm 1}) - 1/2(J_{i, j, k}^{-1} + J_{i, j, k \pm 1}^{-1})d_{i, j, k \pm 1/2}. \end{aligned} \quad (16)$$

In Eqs. (16), the terms $d_{i \pm 1/2, j, k}$, $d_{i, j \pm 1/2, k}$ e $d_{i, j, k \pm 1/2}$ represent the artificial dissipation components in the i, j and k directions, respectively. Equation (1), after complete space discretization, can be rewritten as:

$$\left(\frac{\partial \bar{Q}}{\partial \tau} \right)_{i, j, k} = -RHS_{i, j, k}, \quad (17)$$

where the residue RHS is given by:

$$\begin{aligned} RHS_{i, j, k} &= \frac{1}{\Delta \eta} \left(F_{i+1/2, j, k} - \bar{F}_{v_{i+1/2, j, k}} - F_{i-1/2, j, k} + \bar{F}_{v_{i-1/2, j, k}} \right) + \frac{1}{\Delta \zeta} \left(G_{i+1/2, j, k} - \bar{G}_{v_{i+1/2, j, k}} - G_{i-1/2, j, k} + \bar{G}_{v_{i-1/2, j, k}} \right) \\ &+ \frac{1}{\Delta \xi} \left(E_{i+1/2, j, k} - \bar{E}_{v_{i+1/2, j, k}} - E_{i-1/2, j, k} + \bar{E}_{v_{i-1/2, j, k}} \right), \end{aligned} \quad (18)$$

and $\Delta \xi = \Delta \eta = \Delta \zeta = l$ for the case of general curvilinear coordinates.

According to a multi-stage Runge-Kutta method, the time-marching is given by

$$\bar{Q}_{i, j, k}^{(0)} = \bar{Q}_{i, j, k}^n; \quad \bar{Q}_{i, j, k}^{(l)} = \bar{Q}_{i, j, k}^{(0)} - \alpha_l \cdot \Delta t_{i, j, k} \cdot RHS_{i, j, k}^{(l-1)}, \quad l = 1, 2, \dots, 5; \quad \bar{Q}_{i, j, k}^{n+1} = \bar{Q}_{i, j, k}^{(5)}. \quad (19)$$

In Eqs. (19), the subscripts n and $n+1$ indicate the beginning and the end of the n -th time step, l and $l-1$ represent the Runge-Kutta stage and α_l is the constant of l -th stage. The values used in the present paper are $\alpha_1 = 1/4$, $\alpha_2 = 1/6$, $\alpha_3 = 3/8$, $\alpha_4 = 1/2$ and $\alpha_5 = 1$. The local time step is evaluated by

$$\Delta t_{i,j,k} = \frac{CFL}{c_{i,j,k}}, \quad (20)$$

where the CFL number is kept constant throughout the computational domain. The characteristic speed of propagation of information in the flow, $c_{i,j,k}$, is calculated here as

$$c_{i,j,k} = |q| + a, \quad |q| = \sqrt{u^2 + v^2 + w^2}. \quad (21)$$

As Cruz (2000) described, the artificial dissipation model used in the code is based on the one implemented by Turkel and Vatsa (1994). This is a non-isotropic scalar model, where the coefficients of the artificial dissipation operators terms are functions of the spectral radii of the flux Jacobians matrices. It is also nonlinear and allows the switching between second and fourth difference terms, which is very important in the aim of detecting and adequately capturing shock waves present in the flow. In the longitudinal direction, the artificial dissipation components can be written as:

$$d_{i+1/2,j,k} = \lambda_{i+1/2,j,k} [\mathcal{E}_{i+1/2,j,k}^{(2)} (W_{i+1,j,k} - W_{i,j,k}) - \mathcal{E}_{i+1/2,j,k}^{(4)} (W_{i+2,j,k} - 3W_{i+1,j,k} + 3W_{i,j,k} - W_{i-1,j,k})]. \quad (22)$$

In Eq. (22), the expressions $\mathcal{E}^{(2)}$ e $\mathcal{E}^{(4)}$ are functions of v_i , given by:

$$\begin{aligned} v_i &= \frac{|p_{i+1,j,k} - 2p_{i,j,k} + p_{i-1,j,k}|}{p_{i+1,j,k} + 2p_{i,j,k} + p_{i-1,j,k}}, \\ \mathcal{E}_{i+1/2,j,k}^{(2)} &= k^{(2)} \max(v_{i+1}, v_i), \\ \mathcal{E}_{i+1/2,j,k}^{(4)} &= \max\{0, [k^{(4)} - \mathcal{E}_{i+1/2,j,k}^{(2)}]\}. \end{aligned} \quad (23)$$

The bigger the pressure gradient, the bigger is the v_i value, thus turning on the second difference terms and canceling out the fourth difference ones. This is important for correctly capturing shock waves (see, for instance, Azevedo et. al., 1995, and Turkel and Vatsa, 1994). On the other hand, in smooth regions of the flow, v_i is very small and the second difference terms are turned off, hence maintaining second-order accuracy. The terms $k^{(2)}$ e $k^{(4)}$ are constants and the values adopted for them are those recommended. Hence $k^{(2)}$ e $k^{(4)}$ are $1/2$ e $1/64$, respectively. The W vector is evaluated as follows

$$W = \bar{Q} + [0, 0, 0, p]^T. \quad (24)$$

Analysing Eqs. (25), (2) and (5), one can conclude that the model adopted is coherent to the fact that the total enthalpy must be conserved in Euler flows with stationary downflow conditions.

The scaling factor related to the longitudinal direction is defined as

$$\lambda_{i+1/2,j,k} = \frac{1}{2} [(\bar{\lambda}_\xi)_{i,j,k} + (\bar{\lambda}_\xi)_{i+1,j,k}], \quad (25)$$

where $\bar{\lambda}_\xi$ is evaluated as a function of the flux Jacobian matrices radii in the three directions as follows

$$(\bar{\lambda}_\xi) = (\lambda_\xi) \left[1 + \left(\frac{\lambda_\eta}{\lambda_\xi} \right)^{0,5} + \left(\frac{\lambda_\zeta}{\lambda_\xi} \right)^{0,5} \right]. \quad (26)$$

The spectral radii for the three directions are given by

$$\begin{aligned}
\lambda_{\xi} &= |U| + a\sqrt{\xi_x^2 + \xi_y^2 + \xi_z^2}, \\
\lambda_{\eta} &= |V| + a\sqrt{\eta_x^2 + \eta_y^2 + \eta_z^2}, \\
\lambda_{\zeta} &= |W| + a\sqrt{\zeta_x^2 + \zeta_y^2 + \zeta_z^2}.
\end{aligned} \tag{27}$$

The artificial dissipation components in the others directions are obtained in a completely analogous form.

2.3. Turbulence Models

According to Bigarelli and Azevedo (2002), the turbulence models chosen for the numerical code are based on the Boussinesq hypothesis, which means that the dynamic viscosity coefficient should be replaced by an effective viscosity coefficient which is given by the sum of laminar and turbulent viscosity coefficients. Mathematically, one could write

$$\mu = \mu_L + \mu_T, \tag{28}$$

where the L and T subscripts represent laminar and turbulent coefficients, respectively. Hence, two models originally conceived to aerospace use were selected for the discussed work. One of them is a one-equation model, proposed by Spalart and Almaras (1994), while the other is the SST two-equation model implemented as proposed by Menter (1994).

2.4. Convergence Acceleration Techniques

It was necessary to add to the CFD tool some convergence acceleration techniques, due to the difficulty of obtaining convergence in very refined computational meshes with the present explicit time-marching scheme. Besides the variable time step, given by the definition of the CFL number, multigrid and implicit residual smoothing (IRS) procedure are implemented.

The multigrid technique can provide great convergence acceleration in numerical methods, as shown by Wesseling (1995). The mathematical formulation of this method consists basically in eliminating low frequency errors for very refined meshes solving the problem with coarser ones. This is based on the knowledge that usual time integration methods are more efficient eliminating high frequency errors of a computational mesh, as the error frequency content of a mesh cell is inversely proportional to its volume (Strauss and Azevedo, 2000). The multigrid algorithm adopted in the present code is called full approximation storage (FAS), implemented by Fletcher (1988), which is the recommended method for nonlinear problems. It is based in the exchange of both solution and residue among different mesh levels. Besides, it must be supported by a good time-marching procedure to be effective (Strauss and Azevedo, 2000).

The driving idea of the residue smoothing consists basically of obtaining the residue average of neighboring cells in a certain point, increasing the information exchange among them. In other words, this is a simplified way of adding some implicit relationship in the residue field. This procedure allows the use of higher CFL numbers for the simulations. These averages can be evaluated implicitly or explicitly. The second option is simpler because it uses only known residue values of the neighboring cells involved. The other, on other hand, requires unknown residue values of the neighboring cells, what makes it more expensive, although more efficient. In the present work, a simpler and effective implicit scheme was chosen, as Azevedo (1992) described.

3. Results and Discussion

3.1. Boundary Conditions

The traditional meshes used in computational simulations with the CFD tools of configurations of interest to IAE are basically axisymmetrical and C-shaped, as indicated in Fig. 1. The evolution of the work performed at CTA/IAE demanded a three-dimensional mesh that was obtained with the revolution of the two-dimensional mesh around the symmetry axis. In earlier work, it was chosen to build meshes that represent only half the central body, in order to save computational effort. This was possible due to the symmetry verified in relation to the pitching plane, even in cases with the angle of attack different from zero. In order to take advantage of that, it was necessary to add two azimuthal planes which contained symmetric points to its correspondents on the other side of the symmetry plane in each configuration. The determination of boundary conditions described by Cruz (2000) used most of what had been developed for two-dimensional meshes. This procedure is demonstrated in Fig. 2.

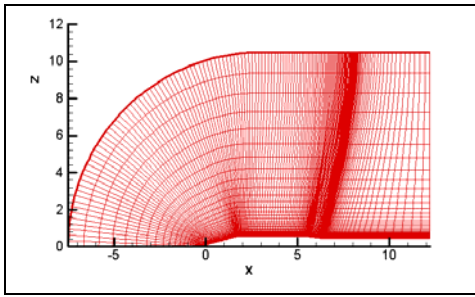


Figure 1. Two-dimensional 155x55 points mesh around SONDA III-A rocket.

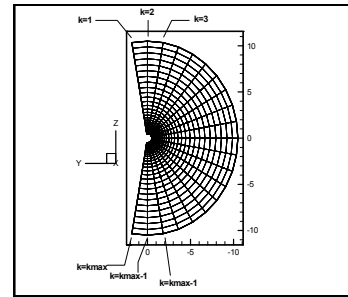


Figure 2. Frontal view of a three-dimensional mesh, evidencing the additional azimuthal planes.

3.2. Mesh Refinement Analysis

The mesh refinement analysis was basically focused in the determination of the number of mesh points in the longitudinal and normal directions of the body. Previous work in the group at CTA/IAE had already established that 21 points are sufficient for the circumferential direction. It is very important to remember that such an analysis was performed with the laminar viscous formulation, without taking into account the turbulent transport phenomena added later to the code. Cases with this more complex formulation demand much more refined meshes. Simulations were, then, performed considering flows around the SONDA III-A rocket with freestream Mach number 2.0, angle of attack 4 deg. and Reynolds number 3×10^7 . Initially, two configurations of mesh were tested: one with $101 \times 34 \times 21$ points and the other with $101 \times 55 \times 21$ points (these numbers refer to the number of grid points in the longitudinal, wall normal and circumferential directions, respectively). The mesh with 34 points in the normal direction was readily discarded due to the large discrepancy in the estimate of the boundary layer thickness comparatively with the mesh with 55 points in that direction.

The following step was to make an analogous experience in order to determine a proper number of mesh points in the longitudinal direction. The possibilities that have already being tested were grid with 101 and 155 points. With a proper control on the distribution of the points, it was possible to verify very similar results for both configurations. Results in terms of pressure contours are shown in Fig. 3, while Fig. 4 contains the pressure coefficient distribution along the vehicle. This makes clear that, with a laminar formulation, the differences between these results are negligible, except for a few points emphasized in Fig. 4. These particular points are located in the regions in which the largest variations occur due to abrupt phenomena. Therefore, within certain limitations, the 101 point mesh can be considered a good compromise demanding much less computational effort than the 155 point mesh.

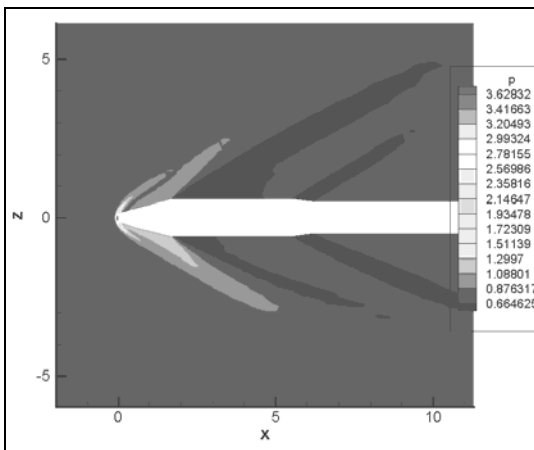


Figure 3. Pressure contour in case Sonda-5 (Table 1) with 4 deg. of angle of attack.

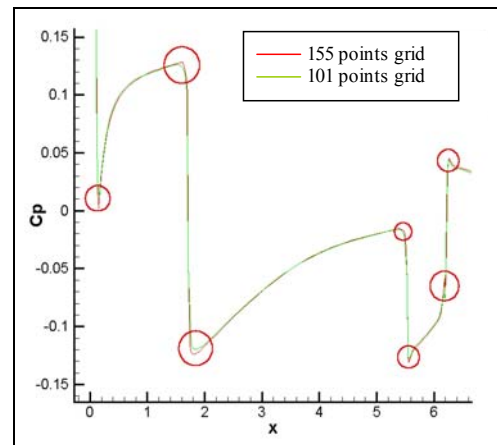


Figure 4. Pressure coefficient distribution for the same conditions.

3.3. Chosen Configurations

As a continuation of an effort to validate the CFD tools developed at CTA/IAE, the present work tried to follow a previously determined simulation schedule with cases of interest. Cruz (2000) presented the complete simulation schedule firstly conceived, but Table 1 contains only the part of interest to this work.

Table 1. Problems selected for simulation and their respective priority.

Case	Geometry/Vehicle	Mach	Attack Angles	Priority
Sonda-4	SONDA III-A	1,25	0, 2, 4 and 6 deg.	High
Sonda-5	SONDA III-A	2,00	0, 2, 4 and 6 deg.	High
Sonda-6	SONDA III-A	3,00	0, 2, 4 and 6 deg.	High
HEM-1	Hemisphere-cilinder	0,90	0	Medium
HEM-2	Hemisphere-cilinder	2,00	0	Medium
HEM-3	Hemisphere-cilinder	5,00	0	Medium
HEM-7	Hemisphere-cilinder	0,90	2, 4 and 6 deg.	Low
HEM-8	Hemisphere-cilinder	2,00	2, 4 and 6 deg.	Low
HEM-9	Hemisphere-cilinder	5,00	2, 4 and 6 deg.	Low

A hemisphere-cilinder body is a geometrically simple problem for which many results are found in the specialized literature. The priority established is related to the lack of time to accomplish completely the schedule determined. All simulations were performed with Reynolds number 3×10^7 . In the interest of brevity, the authors do not include here solutions for all of these cases. However, a calculation which is indicative of the quality of the results obtained in these simulations, without the inclusion of a turbulence model, can be seen in Figs. 3 and 4, which corresponds to the Sonda-5 case in Table 1.

3.4. New Mesh Topology Creation

Among the chosen configurations, the most important ones are in the supersonic regime. However, the mesh topology presented in Fig. 1, developed and used by the CTA/IAE research group, for obvious practical reasons, attempts to cover as many different situations as possible, including subsonic, transonic and supersonic conditions. For this reason, as emphasized by Marques (2002), a new mesh geometry was created aiming to serve exclusively to supersonic cases. The interesting phenomena in this kind of situation are situated after the shock wave detached from the body's nose. Hence, the new topology tries to concentrate the points in this region, without increasing the total number of mesh points and, consequently, the computational effort. This is obtained forcing the external boundary of the mesh to be parallel to the shock wave. After a series of simulations, the proper model was chosen, as described by Marques (2002). The resulting topology is presented in Fig. 5. The savings introduced by this modification showed to be especially important later, when the turbulence models were implemented demanding a further refinement of the mesh.

Another mesh model also had to be generated to create proper conditions for simulations over the hemisphere-cilinder configuration. Due to the lack of time, only a grid adequate for supersonic simulations was developed for this configuration. Figure 6 contains a sample of this mesh.

For illustrative purpose, the result in terms of Mach number contours for the Sonda-4 case, indicated in Table 1, with zero angle of attack using the supersonic mesh topology is shown in Fig.7.

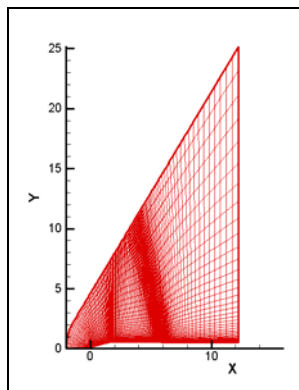


Figure 5. Supersonic case mesh topology. Grid over SONDA III-A rocket.

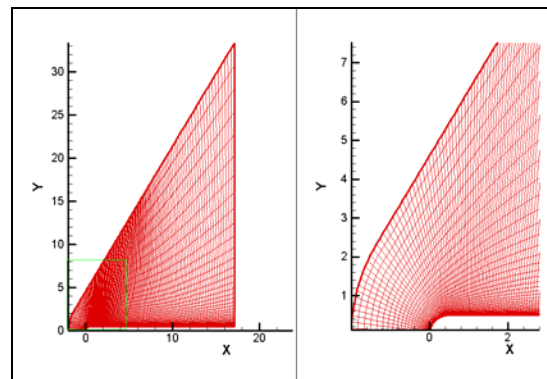


Figure 6. Mesh around a hemisphere-cilinder configuration, including a detail of the nose region.

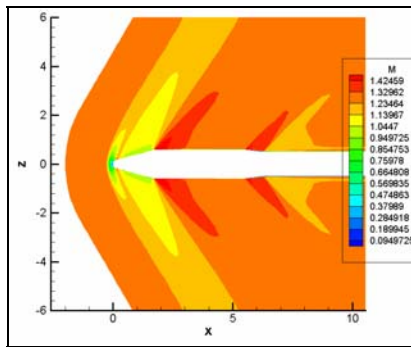


Figure 7. Mach number contour in case Sonda-4 with zero angle of attack.

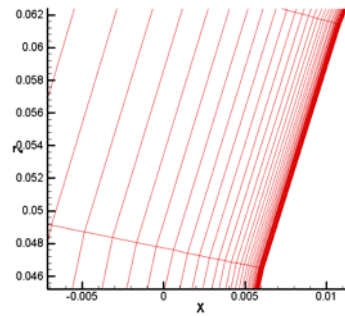


Figure 8. View of the mesh refinement in the nose region.

3.5. Simulations with Turbulence Models

The turbulence models previously cited were added to the numerical code by Bigarelli (2002) during the development of the work of Marques (2002). Thus, in order to take advantage of this evolution, the initial goals were slightly altered to include simulations using the newer formulation at that time. However, in this attempt to obtain more complete e reliable results with the new tool applied to the created mesh topologies, certain difficulties never experienced before by that group emerged. This occurs due to the behavior of the code in very refined regions of the mesh, as the nose of the body

To work properly, the new formulation requires a relatively well-refined mesh, with about 85 to 89 points in the normal direction. These additional points, together with the concentration of points in new meshes, resulted in very stretched cells in the body's proximities, mainly at the nose. Figure 8 shows a sample of this in the SONDA III-A rocket. In some cases, the cell length may be a million times greater than the width. This implies in great challenges to achieve convergence. Figure 9 demonstrates the convergence history in the HEM-2 case with 60,000 multigrid cycles (considered here as iterations), with a very low CFL number of 0.17. These convergence problems were solved with the implementation of the convergence acceleration techniques described in the paper. Figure 10 contains a sample of solution in terms of Mach number contour with these capabilities fully implemented and Figure 11 the corresponding convergence history. This simulation was performed for the VLS configuration because there was more experimental data available. The presented case considers a freestream Mach number 2.0 and 4 deg. of angle of attack. At the present time, the validation effort continues addressing the configurations indicated in Table 1.

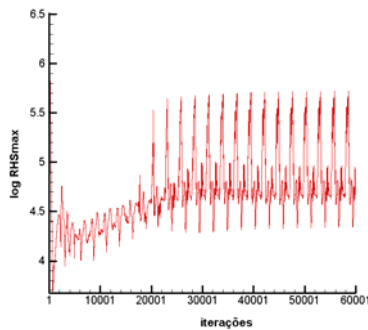


Figure 9. Convergence history for HEM-2 case.

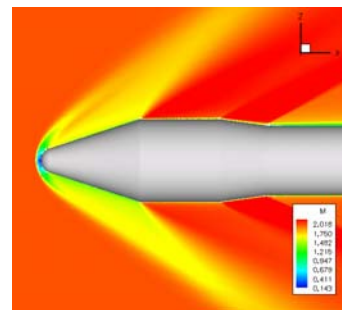


Figure 10. Mach number control around the VLS rocket with $M_\infty = 2.0$ and 4 deg. of angle of attack.

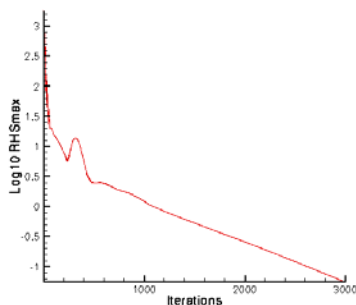


Figure 11. Convergence history for the simulation with the turbulence model and convergence acceleration techniques.

4. Conclusion

This work presents results which contribute to the validation of a CFD simulation tool currently under development at CTA/IAE and ITA, aimed at the solution of high-speed aerospace flows. Some new capabilities have been recently added to this code and it is important to emphasize the addition of turbulence models to the code, as described by Bigarelli and Azevedo (2002). These increase the range of phenomena covered by the CFD tool.

Yet, new mesh topologies are necessary to accomplish the overall development work of which this paper is a part. This task was successfully achieved resulting in new mesh models presented in section 3.4. The simulation schedule presented in section 3.3 could not be completely executed until now for the turbulent case due to unexpected difficulties that emerged during the validation process. Nevertheless, this drove the implementation of advanced convergence acceleration techniques, which made the code more robust. Therefore, the paper has presented results of an on-going work which, however, has already indicated the usefulness of the implemented capability for the flow simulation of interest for aerodynamic analysis of launch vehicles and sounding rockets.

Bibliography

- Azevedo, J.L.F., 1993, "Introdução à Mecânica dos Fluidos Computacional – Notas para Minicurso", XVI Congresso Nacional de Matemática Aplicada e Computacional – CNMAC 93, Uberlândia, MG.
- Azevedo, J.L.F., 1990, "Euler Solutions of Transonic Nozzle Flows", III Encontro Nacional de Ciências Térmicas – III ENCIT, Itapema, SC, pp. 243-248.
- Azevedo, J.L.F., Fico, N.G.C.R., Jr., and Ortega, M.A., 1995, "Two-Dimensional and Axisymmetric Nozzle Flow Computation Using the Euler Equations", Revista Brasileira de Ciências Mecânicas, Vol. 17, N° 2, pp. 147-170.
- Azevedo, J.L.F., Strauss, D., and Ferrari, M.A.S., 1997, "Viscous Multiblock Simulations of Axisymmetric Launch Vehicle Flows", AIAA Paper No. 97-2300, Proc. of 15th AIAA Applied Aerodynamics Conference, Atlanta, GA.
- Azevedo, J.L.F., 1989, "AA290 - Fundamentos de Aerodinâmica Computacional", Notas do Curso AA290, ITA.
- Azevedo, 1992, J.L.F., "On the Development of Unstructured Grid Finite Volume Solvers for High Speed Flows", Technical Note NT-075-ASE-N/72, Instituto de Aeronáutica e Espaço, São José dos Campos, SP, Brazil.
- Bigarelli, E.D.V., Mello, O.A.F., Azevedo, J.L.F., 1999, "Three Dimensional Flow Simulations for Typical Launch Vehicles at Angle of Attack", XV Congresso Brasileiro de Engenharia Mecânica, Águas de Lindóia, SP.
- Bigarelli, E.D.V., and Azevedo, J.L.F., 2002, "On Turbulence Models for 3-D Aerospace Applications" – Proceedings of the 9th Brazilian Congress of Thermal Engineering and Sciences, Paper CIT02-0341, Caxambu, MG.
- Bigarelli, E.D.V., 2002, "Three-Dimensional Turbulent Flows Simulations over Aerospace Configurations", Master's Thesis, Instituto Tecnológico de Aeronáutica, São José dos Campos, SP, Brazil.
- Cruz, L.R.S., 2000, "Simulação de Escoamentos Viscosos sobre Veículos Lançadores", Relatório Final de Bolsa de Iniciação Científica, PIBIC-ITA.
- Fico, N.G.C.R., Jr., and Azevedo, J.L.F., 1994, "Numerical Investigation of Supersonic Flow in a Slotted Wind Tunnel", XV Congresso Ibero Latino-Americano sobre Métodos Computacionais para Engenharia - XV CILAMCE, Belo Horizonte, MG, pp. 314-322.
- Fletcher, C.A.J., 1988, "Computational Techniques for Fluid Dynamics - Fundamental and General Techniques", Vol. I, Springer Verlag, Berlin.
- Fletcher, C.A.J., 1988, "Computational Techniques for Fluid Dynamics - Fundamental and General Techniques", Vol. II, Springer Verlag, Berlin.
- Hirsch, C., 1994, "Numerical Computation of Internal and External Flows - Fundamental of Numerical Discretization", Vol. I, John Wiley & Sons.
- Marques, A.N., 2002, "Validação de Códigos de CFD para Análise Aerodinâmica de Veículos Lançadores e Foguetes de Sondagem", Relatório Parcial de Bolsa de Iniciação Científica, Processo PIBIC-ITA.
- Menter, F.R., 1994, "Two-Equations Eddy-Viscosity Turbulence Models for Engineering Applications", AIAA Journal, Vol. 32, No.8, pp. 1598-1605.
- Spalart, P.R., and Allmaras, S.R., 1994, "A One-Equation Turbulence Model for Aerodynamic Flow", La Recherche Aeropastiale, Vol.1, pp.5-21.
- Strauss, D. and Azevedo, J.L.F., 2000, "Aglomeration Multigrid Solutions of Laminar Viscous Flows", Proceedings of the 8th Brazilian Congress of Thermal Sciences, ENCIT 2000 (Publication in CD-ROM without page numbering).
- Turkel, E., and Vatsa, V.N., 1994, "Effect of Artificial Viscosity on Three-Dimensional Flow Solutions", AIAA Journal, Vol. 32, No. 1, pp. 39-45.
- Wesseling, P., 1995, "Introduction to Multigrid Methods", Tech. Rep. ICASE 95-11, NASA, Langley Research Center, Hampton, VA, USA.